Theoretical Analysis of the Electrochemical Promotion of Infiltrations in MIEC Based Electrodes for IT-SOFCs

Anna Enrico, Paola Costamagna*

Department of Civil, Chemical and Environmental Engineering (DICCA), Polytechnic School, University of Genoa
Via Opera Pia 15, 16145 Genoa, Italy
paola.costamagna@unige.it

We consider mixed ionic-electronic conducting (MIEC) electrodes for intermediate temperature-solid oxide fuel cells (IT-SOFCs). Focusing on the mechanism of charge conduction along the MIEC, we consider that it features two separated charge conduction paths, one for electrons and one for oxygen-ions. Infiltrated nano-sized dopant particles, adherent to the MIEC fibers, create contact points between the ionic and the electronic conductive paths, among which, otherwise, the charge transfer reaction would be negligible.

Based on this picture of the doped MIEC electrode, a model is developed. The model includes the evaluation of i) charge transfer reaction occurring at the dopant particles and, possibly, at the electrode/electrolyte interface; ii) electron and oxygen-ion conduction along the MIEC fiber, and iii) additional charge conduction along the dopant nano-particles, if percolating throughout the electrode structure. The model is applied to $Sm_{0.5}Sr_{0.5}CoO_{3-\delta}$ (SSC) infiltrated $La_{1-x}Sr_xCo_{1-y}Fe_yO_{3-\delta}$ (LSCF) cathodes, and also to Gd-doped CeO_2 (GDC) infiltrated La-doped $SrTiO_3$ (LST) anodes. At 1023 K, an overall reciprocal electrode resistance in the order of $1/R_p \approx 1\times10^6$ S m^{-2} is calculated for the SSC-LSCF cathodes, and $1/R_p \approx 8\times10^3$ S m^{-2} for the GDC-LST anodes. Simulation results are compared to literature experimental data, demonstrating good agreement.

1. Introduction

Traditionally, SOFCs are designed to operate at high temperature (1050-1300 K), which places considerable restrictions on the materials that can be used in both the fuel cell and in the balance of plant (Brett et al. 2008; Tippawan P. et al., 2014). To overcome these problems, IT-SOFCs are currently under development, operating at 750-1100 K. However, lowering the operating temperature also lowers the fuel cell performance, since the kinetics of the electrochemical reaction decreases rapidly as temperature decreases. Furthermore, the electrodes and electrolyte materials become less conductive. Thus, materials with improved conductivity features are being applied (MIECs), and also the morphology is improved through doping with nano-particles, in order to enlarge the active area for the electrochemical reaction.

From a theoretical point of view, the mechanism through which nano-particles improve the performance of MIEC electrodes is not completely clear at present. For this reason, a picture of the chemical-physical phenomena occurring in the electrode is proposed here, which is the basis for the development of a modelling approach. The model is applied to two different types of infiltrated MIEC electrodes, i.e. SSC infiltrated LSCF cathodes, and also GDC infiltrated LST anodes, in order to investigate the mechanism of electrochemical promotion of infiltrated nano-particles.
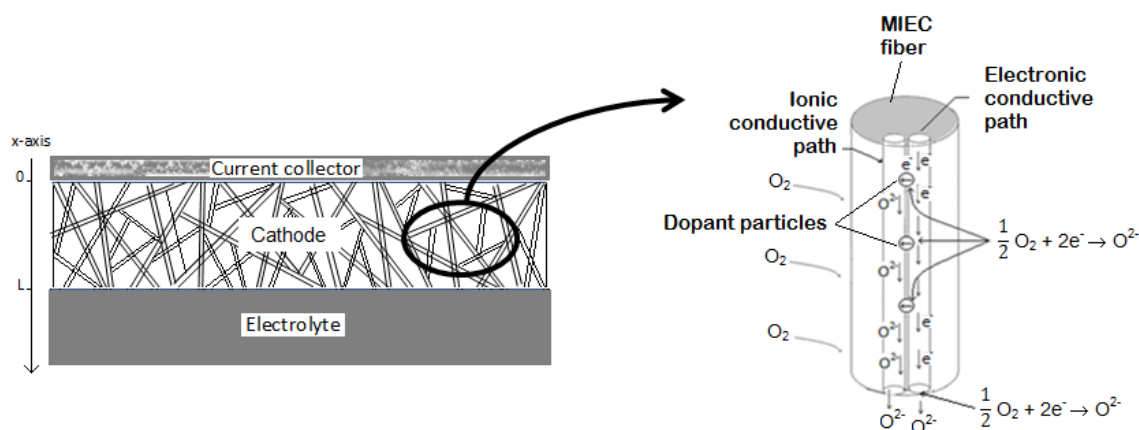
2. Model

Figure 1: Scheme of an infiltrated fibrous MIEC cathode

We take into consideration MIEC electrodes with a fiber-made scaffold. Figure 1 represents a scheme of a fibrous electrode, showing the electrochemical reaction occurring at the cathode: ½ O_2 + $2e^-$ → O^{2-}. At the anode side, the picture is analogous, and the electrochemical reaction is H_2 + O^{2-} → H_2O + $2e^-$. The electrochemical reaction is a charge transfer reaction, i.e. it involves a transfer of electrical charges between the electron conducting and the oxygen-ion conducting paths present in the MIEC fiber, which are displayed in Figure 1 as well. Literature studies demonstrate that in MIEC electrodes, in absence of dopants, the electrochemical reaction occurs mainly at the E/E (electrode/electrolyte) interface, and that the charge transfer reaction away from the E/E interface is almost negligible. In the light of this, we consider that in the pristine MIEC electrode there are conducting paths for electrons and for oxygen-ions, which are separated from each other and, even if they coexist in the MIEC fiber, there are no contact points between them. We suppose that, through the infiltration process, the particles deposited on the electrode scaffold adhere on the surface of the fibers creating contact points between the ionic and the electronic conductive paths. In this way, the addition of infiltrated particles makes it possible the exchange of electrical charges between the two conducting paths, extending the active area for the electrochemical reaction deeply into the electrode thickness, away from the E/E interface, with a consequent improvement of electrochemical performance.

2.1 Model development

The main hypotheses of the model are: 1) DC steady-state operating conditions; 2) temperature and pressure uniform throughout the electrode; 3) the scaffold electrode structure, formed of straight fibers randomly distributed within the electrode, is considered as continuous and homogeneous; 4) in absence of dopants, no charge transfer reaction occurs between the ionic and the electronic conducting paths of the MIEC fibers; 5) dopant particles regularly distributed along the electrode thickness; 6) the whole contact between the dopant particles and the MIEC fibers is assumed to be an active site for the electrochemical reaction; 7) at the E/E boundary, the active site for the electrochemical reaction is assumed to be the whole interface between the electrolyte and the electronic conducting paths of the electrode; 8) hydrogen is the anodic reactant, oxygen the cathode one; 9) mass transport limitations are not taken into account; 10) the model is one-dimensional along the *x*-coordinate which, for the cathode, has its origin at the E/CC (electrode/current collector) boundary and is directed towards the electrolyte (Figure 1); for the anode, the *x*-coordinate has its origin at the E/E boundary and is directed towards the current collector.

The model (Enrico et Costamagna, 2014) is based on the Ohm's law, written under differential form, for the transport of oxygen-ions and electrons, with i_{io} and i_{el} being the ionic and electronic current densities respectively. i_n expresses the electrochemical reaction rate, and is a current density referred to the extension of the area of the active site available for the electrochemical reaction (S_{TPB}, active area per unit volume of the electrode):

$$
\begin{cases}
\dfrac{dV_{io}}{dx} = -\dfrac{i_{io}}{\sigma_{io}^{eff}} \\[2mm]
\dfrac{dV_{el}}{dx} = -\dfrac{i_{el}}{\sigma_{el}^{eff}} \\[2mm]
i_n = i_0\left\{-exp\left(\eta\dfrac{\beta nF}{R_gT}\right) + exp\left[-\eta\dfrac{(1-\beta)nF}{R_gT}\right]\right\} \\[2mm]
\dfrac{di_{io}}{dx} = -\dfrac{di_{el}}{dx} = S_{TPB}i_n \\[2mm]
\eta = (V_{el}-V_{io})^{th} - (V_{el}-V_{io})
\end{cases}
\tag{1}
$$

The electrochemical reaction results in a transfer of charges between i_{io} and i_{el} which, in Eq(1), is expressed through the charge balance equation. Finally, in Eq(1), the definition of overpotential η is recalled. With the choice of the x-axis described in hypothesis 10, these equations apply to both the anode and the cathode. Eq(1) contains a number of parameters, which are evaluated in detail on the basis of literature experimental data (Enrico et Costamagna, 2014). In particular, i_o expresses the kinetics of the electrochemical reaction, and follows the Arrhenius law:

$$
i_0 = K_{kin}\, exp(-\dfrac{E_{a,kin}}{K_BT})
\tag{2}
$$

The conductivities appearing in Eq(1) are the affective ionic and electronic electrode conductivities. These account for the ionic and electronic conductivities of the MIEC fibers, both of which follow the law:

$$
\sigma_{MIEC} = \dfrac{K}{T}\, exp(-\dfrac{E_a}{K_BT})
\tag{3}
$$

In addition, also the infiltrations give a contribution to the charge transport, provided that percolation takes place. Percolation occurs when the infiltrations form an interconnected network through the electrode, spanning throughout the whole electrode thickness. The related conductivity is evaluated through the percolation theory, specifically applied to particles infiltrated into electrode scaffolds (Chen et al., 2013):

$$
\sigma_{inf} = \sigma^0\, \dfrac{(r_p^2 - r_{eq}^2)ln\left[tan\left(\theta_0/2\right)\right]}{r_p r_{eq}cos\alpha_0}\left[\dfrac{\phi_{inf}-P_C}{1-P_C}(1-\varepsilon^{eq})\right]^\gamma
\tag{4}
$$

Where ϕ_{inf} is the volume fraction of infiltrated nano-particles, ε^{eq} is an equivalent electrode porosity, α_0 is the contact angle, θ_0 is a geometrical parameter, γ is the Bruggeman factor which takes into account the tortuosity of the conduction paths, and P_C is the percolation threshold of the infiltrations.

The effective conductivities appearing in Eq(1) are then evaluated by combining among them the MIEC conductivities σ_{MIEC} (ionic and electronic) and the conductivity of the infiltrations σ_{inf}.

Boundary condition for the system of equations reported above is the overall operating electrode current density I_{tot}. The model equations are integrated trough MATLAB®.

3. Model results

The model allows to evaluate: 1) some electrode features, in particular the effective ionic conductivity, as a function of the electrode composition and morphology; 2) the distributions of current density and voltage along both the electronic and ionic conducting paths spanning throughout the whole electrode thickness; and 3) the overall electrode performance, which is summarized through the parameters $1/R_p$ and EAT (Electrochemically Active Thickness). $1/R_p$ is the reciprocal overall electrode resistance, accounting for all sources of voltage loss, including electrochemical reaction and charge transport through the electrode. The EAT (Fan et al., 2014) is defined as the electrode thickness close to the E/E interface where 95 % of the electrochemical reaction takes place (Enrico et al., 2014).

3.1 SSC infiltrated LSCF cathodes, with low infiltration loads ($n_P/L < 20$)

Table 1a: Model parameters for SSC-LSCF cathodes	
k_{io} [S K m^{-1}], $E_{a,io}$ [J]	1.72x10^9, 1.97x10^{-19}
k_{el} [S K m^{-1}], $E_{a,el}$ [J]	1.52x10^8, 1.82x10^{-20}
k_{kin} [S m^{-2}], $E_{a,kin}$ [J/mol]	6.08x10^{14}, 1.32x10^5

Table 1b: Model parameters for GDC-LST anodes	
k_{io} [S K m^{-1}], $E_{a,io}$ [J]	1.09x10^6, 8.01x10^3
k_{el} [S K m^{-1}], $E_{a,el}$ [J]	1.08x10^5, 3.91x10^3
k_{kin} [S m^{-2}], $E_{a,kin}$ [J/mol]	1.18x10^{14}, 1.83x10^6

We apply our model to literature SSC infiltrated LSCF cathodes (Lou et al., 2009), obtained through a one-step infiltration process with a concentration of the infiltrated solution varying from 0.16 mol/L to 1.44 mol/L of SSC. We consider the cathode as fiber-made, even if the electrode scaffold is formed of sintered LSCF naparticles (size 200 nm). Indeed, TEM analyses (Fan et al., 2013) show that during the heat treatment, the nanoparticles often join losing their starting shape and forming nanofibers. Geometrical parameters are derived from the literature (Lou et al., 2009), as well as the parameters for the evaluation of the MIEC conductivities and electro-kinetics, which are reported in Table 1a.
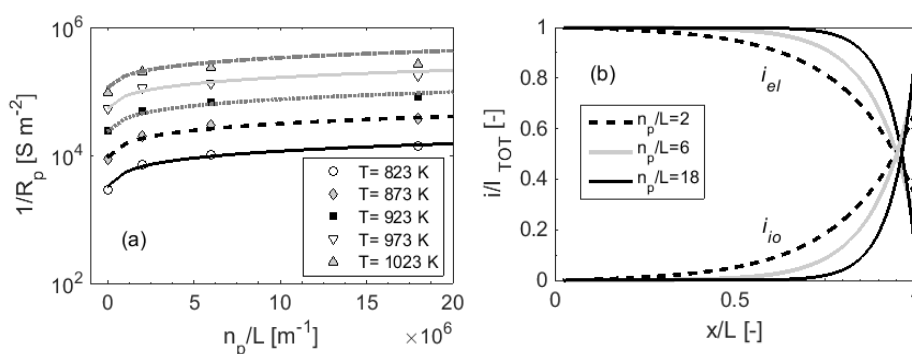

Figure 2: SSC infiltrated LSCF cathodes (electrolyte: GDC): (a) Reciprocal electrode resistance as a function of the infiltration load n_p/L. Symbols: literature experimental data (Lou et al., 2009). Lines: model simulations. (b) Simulated ionic and electronic current densities along the x-coordinate (T= 1,023 K and I_{TOT} = 3,000 A m^{-2})

Figure 2a shows simulation results together with literature experimental data (Lou et al., 2009) as a function of the infiltration load n_p/L (number of particles per unit thickness of the electrode), at various operating temperatures in the range 823-1,023 K. We have evaluated an infiltration load n_p/L = 2 particles/µm for an experimental doping level of 7 µL of infiltrated solution containing 0.16 mol/L of SSC. The increased amounts of dopant particles are evaluated by increasing n_p/L proportionally to the concentration of the infiltrating solution. The maximum simulated value of n_p/L is 18 particles/µm, which, taking into account that each particle has a diameter of 20-30 nm, can be considered as a low infiltration load, far below percolation. Thus, the presence of infiltrations is neglected in the evaluation of the effective electrode conductivities, which accounts only for the MIEC ionic and electronic conductivities.

Figure 2a demonstrates a good agreement between simulation results and literature experimental data. The results show that an increased operating temperature enhances the electrode performance, and this is due to the increased electrochemical kinetics and charge transport. Also the increase of electrode doping level enhances the electrode performance, and this is further investigated, on the basis of simulation results, in Figure 2b, which displays the distributions of electronic and ionic currents for infiltrated electrodes with three different levels of doping. In all cases, the electronic current i_{el} decreases along the electrode thickness due to the electrochemical reaction occurring at each doping particle; in parallel, the ionic current density i_{io} increases. These simulation results indicate that the electrochemical reaction mostly occurs in an electrode region adjacent to the electrolyte, whose thickness is the *EAT* reported in Table 2a. Figure 2b and Table 2a show that, increasing the infiltration loading, the reaction gets concentrated closer to the E/E interface, resulting in a decrease of the *EAT*. This is explained considering that, in this situation, where the oxygen-ion transfer along the electrode thickness is one of the rate determining steps of the phenomenon, an increase of the doping level does not affect the ionic conductivity (which is the conductivity of the pristine MIEC cathode). On the other hand, when increasing of the doping level n_p/L, the number of active sites available for the electrochemical reaction per unit thickness of the electrode is enhanced. As a consequence, the electrochemical reaction develops in a region closer to the E/E interface, corresponding to a shrinking of the

EAT, with a shorter path of the oxygen-ions within the electrode. This effect is beneficial, as displayed by Table 2a, which shows that this is associated to an increase of $1/R_p$ when increasing of the doping level n_p/L.

Table 2a: Model results for SSC-LSCF cathodes (T=1023 K)

n_p/L [m^{-6}]	σ_{io}^{eff} [S m^{-1}]	$1/R_p$[S m^{-2}]	EAT [10^{-6} m]
2	1.713	5.96x10^5	22.50
6	1.713	8.89 x10^5	12.5
18	1.713	1.4x10^6	10.6

Table 2b: Model results for GDC-LST anodes (T=1023 K)

n_p/L [m^{-6}]	σ_{io}^{eff} [S m^{-1}]	$1/R_p$ [S m^{-2}]	EAT [10^{-6} m]
84	0.012	2.61 x10^3	15
93.5	0.050	5.48x10^3	30.12
118	0.108	8.05 x10^3	38.77

3.2 GDC infiltrated LST anodes, with high infiltration loadings (np/L > 80)

We apply our model to literature fibrous LST anodes infiltrated with GDC (Fan et al., 2014), coupled to ScSZ ((ZrO$_2$)$_{1-x}$(Sc$_2$O$_3$)$_x$) electrolytes. The fibrous LST scaffolds, manufactured through electrospinning, provide the electrodes with adequate robustness, and also build highly electronic conductive three-dimensional paths. High loadings of GDC infiltrations are easily accommodated into the highly porous starting fibrous scaffolds.

As far as the model parameters are concerned, geometrical parameters have been derived from the literature (Fan et al., 2014), as well as the parameters for the evaluation of the MIEC conductivities and electro-kinetics, which are reported in Table 1b. In the literature experimental electrodes, the mass ratio of GDC to LST is varied from 0.5 to 1.3 w/w, which corresponds to a volume fraction varying from around 29 % to around 52 % (referring to the total solid volume, voids excluded). Considering that, with infiltrated nano-particles of 20-30 nm diameter, percolation occurs for a volumetric fraction of the infiltrations of 10 % (voids excluded) (Chen et al., 2013), the infiltration loads under consideration are above the percolation threshold. Therefore, the effective ionic conductivity of the electrode is then calculated through the model taking into account the percolation of the infiltrated particles, expressed by Eq(4).
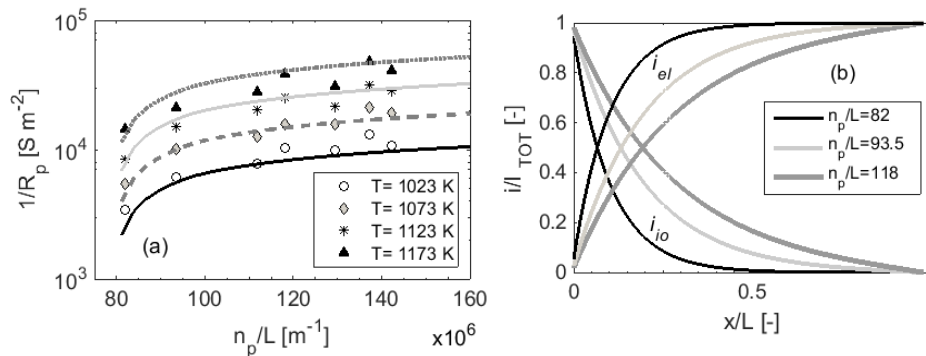

Figure 3: GDC infiltrated LST anodes (electrolyte: ScSZ): (a) Reciprocal electrode resistance as a function of the infiltration load n_p/L. Symbols: literature experimental data (Fan et al., 2014). Lines: model simulations. (b) Simulated ionic and electronic current densities along the x-coordinate (T= 1,023 K and I$_{TOT}$=3,000 A m^{-2})

Figure 3a shows simulation results together with literature experimental data as a function of n_p/L, at various operating temperatures in the range 1023-1173 K. We assume that a volume fraction of 29.8% of infiltrated GDC corresponds to n_p/L =82 particles/μm. For higher doping levels, n_p/L has been increased proportionally to the amount of infiltrated particles reported in the literature.

Also here, the results show that by increasing the operating temperature or the infiltration level the simulated electrode performance increases, displaying good agreement with the literature experimental data. Figure 3b shows that, in this case, when the infiltration level increases, then the region where the electrochemical reaction occurs expands. This is confirmed by the increase of the *EAT* reported in Table 2b. This result is opposite to that reported in Section 3.1. for SSC infiltrated LSCF cathodes. This difference is explained considering the increase of the effective ionic conductivity of the GDC-LST anode (reported in Table 2b), obtained when the infiltration load increases, which is related to an increase of connectivity among the percolating infiltrated particles. In this case, the increasing infiltration load has two simultaneous positive effects, i.e. an increase of the active sites available for the electrochemical reaction per unit thickness of the

electrode, and also an enhancement of the oxygen-ion conduction throug the electrode. As a consequence of this latter effect, the oxygen ions, coming from the electrolyte, are more efficiently transferred inside the electrode thickness and undergo electrochemical reaction more deeply inside the electrode, and this is the reason for the increase of the *EAT*.

As a final remark, the GDC-LST anodes simulated in this study have effective ionic conductivity (Table 2) and also electro-kinetics parameters (Table 1) inferior to those of the state-of-the-art Ni-based cermets, and also worse than those of the SSC-LSCF cathodes considered in the present work, and consequently their electrochemical performance ($1/R_p$) is lower.

4. Conclusions

We analyse the role of infiltrations into IT-SOFC electrodes through a modelling approach. The model results emphasize that the presence of infiltrations allows the electrochemical reaction to extend into the electrode thickness. The overall electrode performance, summarized through the parameter $1/R_p$, is demonstrated to increase when increasing the infiltration level n_p/L. However, the mechanism is different, depending whether the amount of infiltrated particles is above or below the percolation threshold. Our results demonstrate that, if the amount of infiltrations is below percolation, then an increase of the dopant load leads to a reduction of the *EAT*, i.e. to a concentration of the electrochemical reaction close to the E/E boundary, accompanied by an increase of $1/R_p$. On the other hand, if percolation occurs among the dopants, then an increased transport of charged species through the percolating particles occurs. This latter effect can change drastically the distribution of the electrochemical reaction, which penetrates further away from the E/E boundary, with an increase of the *EAT* and, again, with an increase of $1/R_{p,,}$ which is more marked than in the case where percolation does not occur.

Our results suggest that high levels of infiltration are recommended. However, at very high infiltration levels, mass transport limitations can arise due to occlusion of the electrode pores. The amount of dopant particles which can be accommodated into the electrodes depends on the pristine electrode structure: from this point of view, fibrous electrodes are preferable since they offer a higher void degree compared to pristine electrodes manufactured through powder sintering.

Our modelling approach is applied to SSC infiltrated LSCF cathodes, and also to GDC infiltrated LST anodes. At 1023 K, an overall reciprocal resistance in the order of $1/R_p \approx 1 \times 10^6$ Sm^{-2} is calculated for the previous ones, and $1/R_p \approx 8 \times 10^3$ Sm^{-2} for the latter. Such values are confirmed by the available literature experimental data, and are promising in view of IT-SOFC applications.

References

Brett D.J.L., Atkinson A., Brandon N.P., Skinnerd S.J., 2008, Intermediate temperature solid oxide fuel cells. Chemical Society Reviews, 37 (8), 1568-1578

Chen M., Liu T., Lin Z., 2013, Theory for the Electrical Conductivity of Nanoparticle-Infiltrated Composite Electrode of Solid Oxide Fuel Cell. ECS Electrochemistry Letters, 2(11), F82-F84.

Enrico A., Cannarozzo M., Costamagna P., 2014, Modeling Analysis of Bi-Layer Ni-$(ZrO_2)_x(Y_2O_3)_{1-x}$ Anodes for Anode-Supported Intermediate Temperature-Solid Oxide Fuel Cells. Energies 7(9), 5647-5674.

Enrico A., Costamagna P., 2014, Model of an infiltrated $La_{1-x}Sr_xCo_{1-y}Fe_yO_{3-\delta}$ cathode for intermediate temperature solid oxide fuel cells. Journal of Power Sources, 272, 1106-1121.

Fan L., Xiong Y., Liu L., Wang Y., Brito M. E., 2013, Preparation and Performance Study of One-Dimensional Nanofiber-Based $Sm_{0.5}Sr_{0.5}CoO_{3-\delta}$-$Gd_{0.2}Ce_{0.8}O_{1.9}$ Composite Cathodes for Intermediate Temperature Solid Oxide Fuel Cells. International Journal of Electrochemical Science 8, 8603-8613

Fan L., Xiong Y., Liu L., Wang Y., Kishimoto H., Yamaji K., Horita T., 2014, Performance of $Gd_{0.2}Ce_{0.8}O_{1.9}$ infiltrated $La_{0.2}Sr_{0.8}TiO_3$ nanofiber scaffold as anode for solid oxide fuel cells. Journal of Power Sources 265, 125-131.

Lou X., Wang S., Liu Z., Yang L., Liu M., 2009, Improving $La_{0.6}Sr_{0.4}Co_{0.2}Fe_{0.8}O_{3-\delta}$ cathode performance by infiltration of a $Sm_{0.5}Sr_{0.5}CoO_{3-\delta}$ coating. Solid State Ionics, 180, 1285-1289.

Tippawan P., Assabumrungrat S., Arpornwichanop A., 2014, Theoretical study on the ethanol-fueled SOFC system integrated with dehumidifier. Chemical Engineering Transactions, 39, 1465-1470.

Zheng K., Li L., Ni M., 2014, Investigation of the electrochemical active thickness of solid oxide fuel cell anode. International Journal Hydrogen Energy, 39, 12904–12912.